Polygonal Functional Expansion Tallies Using Transformed Zernike Polynomials

Joseph F. Specht IV [1,*], April J. Novak[1]

[1]University of Illinois, Urbana-Champaign, Illinois

[leave space for DOI, which will be inserted by ANS]

ABSTRACT

In Monte Carlo neutron transport, tallies are used to score reaction rates and particle flux. Currently available tallies in OpenMC include: (i) cell tallies, which can be tedious to construct for spatial resolutions smaller than the cells used to build geometry; (ii) mesh tallies, which may result in high bin counts to be conformal to geometry; and (iii) functional expansion tallies. Functional expansion tallies are characterized by low user effort to establish and, for certain geometries, geometric conformity. However, the existing orthogonal polynomials used for functional expansion tallies are only applicable over specific geometries, such as lines, disks, and spheres. Therefore, this paper introduces the notion of functional expansion tallies over arbitrary polygons, and implements this capability into the OpenMC Monte Carlo code. These polygon functional expansion tallies employ a transformed Zernike polynomial which form an orthogonal set of functions on n-sided regular polygons. This paper describes the theory of polygon functional expansion tallies and applies the method to several test cases. First, preliminary testing shows polygon function expansion tallies represent functions with more than an order of magnitude less error than Zernike function expansion tallies. Next, polygon function expansion tallies are added into OpenMC and compared with Zernike function tallies. Each function expansion tally is compared to a reference distributed cell tally. From this comparison, polygonal function expansion tallies are best used on polygonal domains to represent fairly discontinuous functions. However, standard Zernike function expansion tallies are best used for smooth, continuous functions, such as flux.

Keywords: Functional Expansion Tally, Tallies, OpenMC, Zernike Polynomials, Monte Carlo

1. INTRODUCTION

Scoring reaction rates and flux is essential for reactor design and analysis, and Monte Carlo neutron transport codes are one method nuclear engineers predict these quantities. One such neutron transport code is OpenMC [1], a Monte Carlo neutron and photon transport code. OpenMC tallies consist of two parts: the score, which specifies the reaction; and the filter, which specifies a region of phase space (possibly in addition to other filters like energy bins).

Currently, OpenMC supports cell, mesh, and functional expansion spatial filters. Cell filters conform to the geometry, but require high user effort – the user manually splits the cell of interest into "sub-cells" with each sub-cell being tallied individually. Mesh filters are the most general, applying to any geometry, but generally use first-order elements, which may not be geometrically conformal when curves are present – improving conformity for mesh filters typically results in high bin counts. By comparison, functional expansion tallys

*jspecht3@illinois.edu

(FETs) have few downsides: low user effort, (potentially) lower computational cost for smooth solutions, and geometric conformity. However, a significant downside of FETs is their limitation to geometries where the polynomial functions are orthogonal, such as lines, disks, and spheres.

FETs represent a quantity of interest as a series expansion using a set of orthogonal basis functions scaled by expansion coefficients [2]. The basis functions chosen for the FET determine the domain over which the FET is orthogonal. In OpenMC, the supported FETs correspond to three sets of basis functions: Legendre polynomials, spherical harmonics, and Zernike polynomials. With Legendre polynomials being orthogonal on the line from $[-1, 1]$, spherical harmonics being orthogonal over the surface of the unit sphere, and Zernike polynomials being orthogonal over the unit disk.

As a result, currently implemented FETs can represent simple geometries, including: cylindrical pincells, parallelepipeds, and spheres. However, currently implemented FETs cannot perfectly represent polygonal geometries well due to non-conformity with the geometry. The downsides of existing FETs motivated the implementation of polygon FETs, which are orthogonal over n-sided polygons.

Potential applications of polygon FETs include the cores of High Temperature Gas Reactors (HTGRs) and sodium fast reactors (SFRs), whose fuel bundles are hexagonal in shape. Both of these reactors are well-suited for tallying power and flux using hexagonal polygon FETs (one tally per bundle) due to the moderate to high mean free path, resulting in fairly smooth tally distributions. In principle, the methods discussed in this paper can also be applied to irregular polygons, such as in unstructured meshes, a topic to be pursued in our future work.

This paper first describes standard Zernike polynomials (Sec. 2.1) and Zernike-like polynomials (Sec. 2.2), which are orthonormal over regular polygons. Next, a proof-of-concept (Sec. 3) was studied using a sandboxed Python code, which showed great promise and motivated the implementation of FETs into OpenMC. Then, an OpenMC model (Sec. 4) was used to compare distributed cell tallies, Zernike FETs, and polygon FETs. Finally, the OpenMC results and comparison of the different tallies (Sec. 5). Finally, an outlook on future work is described in Section 6.

2. ZERNIKE POLYNOMIALS

2.1. Zernike Polynomials

The Zernike polynomials are a family of polynomials orthonormal over the unit disk with respect to the Lebesgue measure $\rho d\rho d\phi/\pi$ such that [3]:

$$\int_0^{2\pi}\int_0^1 Z_{n_1}^{m_1}(\rho,\phi)\cdot Z_{n_2}^{m_2}(\rho,\phi)\frac{\rho d\rho d\phi}{\pi} = \left\{ \begin{array}{ll} 0, & n_1 \neq n_2 \ \vee \ m_1 \neq m_2, \\ 1, & n_1 = n_2 \ \wedge \ m_1 = m_2. \end{array} \right\}, \tag{1}$$

where Z_n^m is the Zernike polynomial of radial order n and azimuthal order m with ρ, ϕ being the standard polar coordinates of the unit disk. The radial order n is an integer that ranges from $[0, \infty)$. Each n has a corresponding set of azimuthal orders m with the set having a size of $n + 1$. All valid m for a given n is given by the sum $\sum_{i=0}^{n} -n + 2i$. The standard definition of Z_n^m is given as [3]:

$$Z_n^m(\rho,\phi) \equiv \left\{ \begin{array}{ll} N_n^m R_n^{|m|}(\rho)\cos(m\phi), & m \geq 0 \\ -N_n^m R_n^{|m|}(\rho)\sin(m\phi), & m < 0 \end{array} \right\}, \tag{2a}$$

$$R_n^{|m|}(\rho) \equiv \sum_{k=0}^{\frac{n-|m|}{2}} \frac{(-1)^k (n-k)!}{k! \left(\frac{n+|m|}{2}-k\right)! \left(\frac{n-|m|}{2}-k\right)!} \rho^{n-2k}, \tag{2b}$$

$$N_n^m \equiv \sqrt{\frac{2(n+1)}{1+\delta_{m,0}}}. \tag{2c}$$

The standard Zernike polynomials are orthonormal over the unit disk, however, most disks do not have a radius of unity. As such, a new family of Zernike-like polynomials, orthogonal over non-unit disks of radius R_0, are defined as:

$$\bar{Z}_n^m(r,\theta) = Z_n^m\left(\frac{r}{R_0}, \theta\right), \tag{3}$$

where r, θ are the polar coordinates on any non-unit disk. Equation 3 normalizes r by the radius of the non-unit disk R_0 such that $0 \leq \frac{r}{R_0} = \rho \leq 1$. With r normalized, the Zernike polynomials are orthogonal over any disk.

2.2. Zernike Polynomials on Regular Polygons

Currently, OpenMC generates Zernike FETs for two-dimensional, circular geometries using the functions $\bar{Z}_n^m$ (Eq. 3), which allows FET expansion over any circular domain. To generate a family of polynomials orthogonal over any regular polygon, a similar transformation to the non-unit-disk radial-coordinate normalization is applied. However, the notion of an R_0 is more complicated in a regular polygon as the polygon radius is now a function of the polar coordinate on the regular polygon θ. To transform a regular polygon to the unit disk, the polygon radius r needs to be normalized such that $\{0 \leq \frac{r}{R_\alpha(\theta)} = \rho \leq 1\}$, $\forall\ \theta$. In these transformed Zernike polynomials, $R_\alpha(\theta)$ is the upper bound of the radial coordinate interval at a given θ. The variable radius R_α is defined as follows [4]:

$$R_\alpha(\theta) \equiv \frac{R_0 \cos(\alpha)}{\cos(U_\alpha(\theta))}, \tag{4a}$$

$$U_\alpha(\theta) \equiv \theta - \left\lfloor \frac{\theta+\alpha}{2\alpha} \right\rfloor 2\alpha, \quad 0 \leq \theta < 2\pi. \tag{4b}$$

where R_0 is the radius of the polygon, α is defined as π/p, and p is the number of sides of the polygon. Both R_α and U_α are periodic with a period of 2α or the angle spanned by a polygon sector. U_α is a function that tracks the depth into the current sector. Both R_α and U_α are shown for a square in Fig. 1.
With R_α and U_α, the Zernike polynomials can be transformed into a family of polynomials orthogonal over the unit disk [4]:

$$K_n^m(r,\theta) = Z_n^m\left(\frac{r}{R_\alpha(\theta)}, \theta\right). \tag{5}$$

Equation 5 maps the domain of a regular polygon to the unit disk, thus generating a family of Zernike-like polynomials geometrically conformal to and orthogonal over any regular polygon. With the theory laid out, these K_n^m functions enable the implementation of polygon FETs into OpenMC.

3. PROOF-OF-CONCEPT

Before implementing polygon FETs into OpenMC, preliminary testing verifies the use of K_n^m to represent polygonal spatial distributions. Henceforth, the family of polynomials $\bar{Z}_n^m$ (Eq. 3) are referred to as the "Z basis" (the untransformed Zernike polynomials) and the family of polynomials K_n^m (Eq. 5) are referred to as

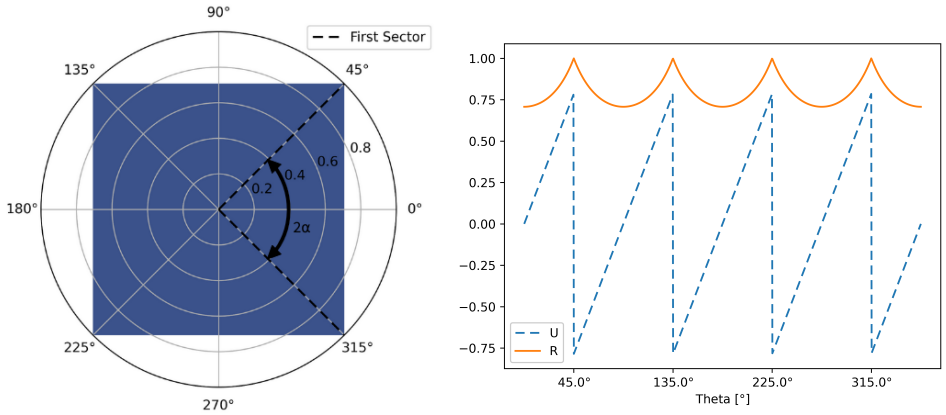

(a) Fist sector and α. **(b) R_α and U_α**

Figure 1. Variable radius and associated quantities for a square, $p = 4$.

the "K basis" (the polygonal Zernike polynomials). The metric of comparison is the difference in relative L^2 norms between the approximation and various analytical functions – this difference in norms is referred to as "error" throughout.

3.1. Overview

To begin, the applicability of the K basis for approximating functions over polygons is tested – a function, defined over a polygon, is approximated using the Z and K bases. The untransformed, Z basis, will be built using a circle circumscribing the polygon. The error of each approximation is then calculated and compared. A function F can be represented in terms of the Z basis as [4]:

$$F(r,\theta) = \sum_{n=0}^{\infty} \sum_{m=-n}^{n} z_n^m \bar{Z}_n^m \left(\frac{r}{R_0}, \theta\right), \tag{6a}$$

$$z_n^m \equiv \int_0^{2\pi} \int_0^{R_0} F(r,\theta) \bar{Z}_n^m \left(\frac{r}{R_0}, \theta\right) \frac{r\,dr\,d\theta}{\pi R_0^2}. \tag{6b}$$

Similarly, a function F in terms of the K basis is given as [4]:

$$F(r,\theta) = \sum_{n=0}^{\infty} \sum_{m=-n}^{n} k_n^m K_n^m \left(\frac{r}{R_\alpha}, \theta\right), \tag{7a}$$

$$k_n^m \equiv \int_0^{2\pi} \int_0^{R_\alpha} F(r,\theta) K_n^m \left(\frac{r}{R_\alpha}, \theta\right) \frac{r\,dr\,d\theta}{\pi R_\alpha^2}. \tag{7b}$$

Next, the errors of each approximation are compared to quantify their accuracy. As the domain under investigation is a regular polygon, the Z basis vectors are not orthogonal over the domain. Conversely, the K basis vectors are orthonormal over the domain. As the Z basis is also non-conformal to the problem geometry, there are unused regions of the Z basis, pictured in Fig. 2, which will increase error.

3.2. Mesh Size Investigation

Before comparing the Z and K bases, the convergence properties of the K basis is investigated. During the proof-of-concept, the coordinates ρ and ϕ are divided into M equally spaced elements. The coordinates ρ

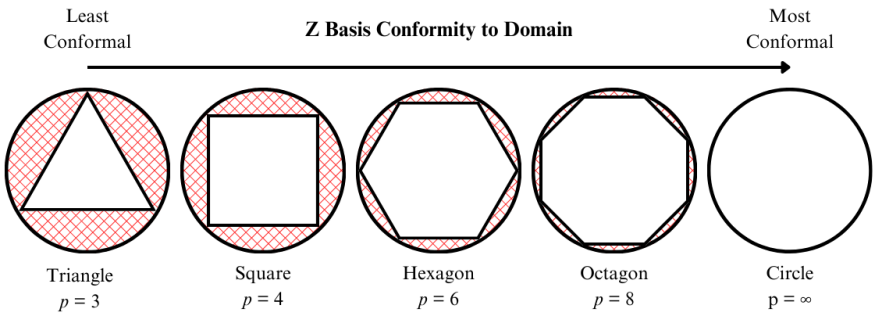

Figure 2. Conformity of Z basis to various p-sided polygons.

and ϕ are used to generate a mesh over the unit disk. Next, the unit-disk mesh is transformed into a mesh over the regular polygon. An informed choice of M is necessary for error convergence as, if M was too small, the error in numerical integration (analogous to statistical error from OpenMC once these methods are implemented into OpenMC) will dominate the truncation error reduction [2].

Then, a function is approximated using the K basis for various M. The function used for testing is

$$f(x, y) = 2x^3 - y^2 + x^2y - 4xy^2 + 5xy - 3x + 5y. \tag{8}$$

This function is sufficiently complicated as to not be represented with a trivial number of terms. From each approximation, the error is calculated and plotted in Fig. 3. As seen in Fig. 3, an M less than 2500 results in divergent error below a Zernike radial order of 20. Therefore, an M value high enough to obtain convergent error is used for the basis comparisons. Again, this is analogous to having sufficiently accurate numerical integration.

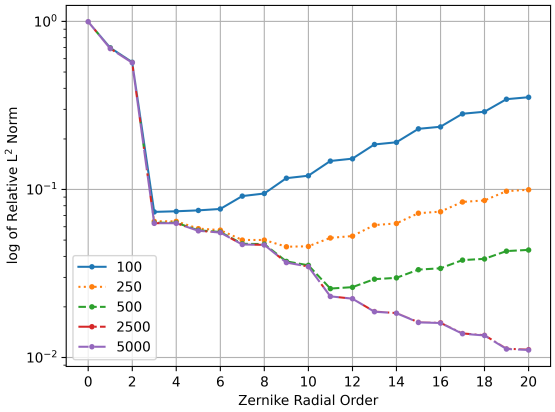

Figure 3. Effect of the number of mesh elements on error for K Basis.

3.3. Different Polygons

Next, the Z and K bases are used to approximate the same function (Eq. 8) as earlier. In this investigation, the function is unchanged and a constant M of 5000 is used. However, the number of sides on the polygon over which the function is approximated is changed. Five polygons are tested, but only the triangle and icosagon, a 20-sided polygon, are shown as these shapes are, respectively, the least and most conformal to the domain of the Z basis of those tested. The errors for each polygon are calculated until the 35th Zernike radial order for each basis and pictured after the individual comparisons on the triangle and icosagon in Fig. 6.

For the first comparison, the function (Eq. 8) is defined over a triangle and approximated with the Z and K bases. The triangle is the polygon with the most apparent differences between the Z and K approximations. The K basis approximates each polygon consistently well, but the Z basis does not. As the triangle only covers 41.4% of the Z basis domain, the Z basis approximation is very poor. In Fig. 4, the approximations over the triangle for both bases are pictured along with the analytical function. It is possible that using barycentric coordinates with conventional Legendre FETs would be an alternative approach to use FETs on triangles, which will be explored in future work.

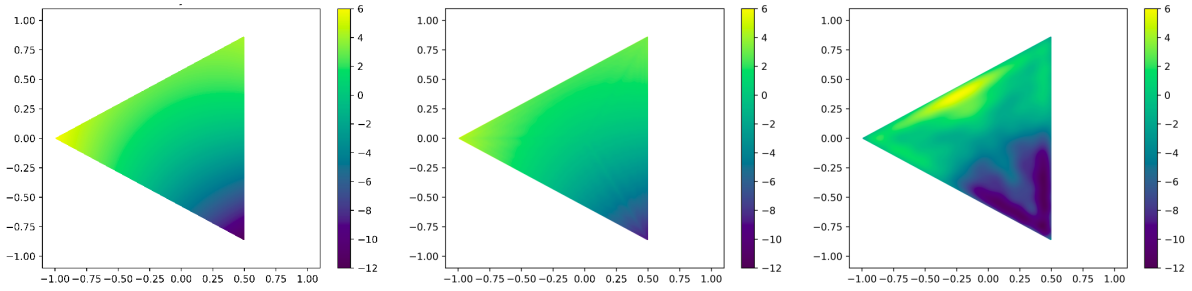

(a) Analytical function **(b) K basis approximation** **(c) Z basis approximation**

Figure 4. Difference in K and Z bases compared to the analytical function on a triangle.

As seen in Fig. 4, the polygon FET (K-basis) approximates the analytic function better than the circumscribed FET (Z-basis). Although the K basis is very accurate, there are visible distortions in every approximation. These distortions manifest as "webbing" near the polygon radii. The webbing is a consequence of the transformation and is more severe at lower Zernike radial orders and lower p. Since the local radius r, which is smooth, is normalized by R_α, which is not smooth, the ratio of the two is not smooth and follows a trend similar to R_α in Fig. 1.

The Z basis performs far better on the icosagon than the triangle as the area of the icosagon covers 98.4% of the Z basis. The K basis also performs better on the icosagon as the ratio between the minimum and maximum R_α is higher than the triangle resulting in less severe webbing. The analytical function with the Z and K bases are pictured in Fig. 5.

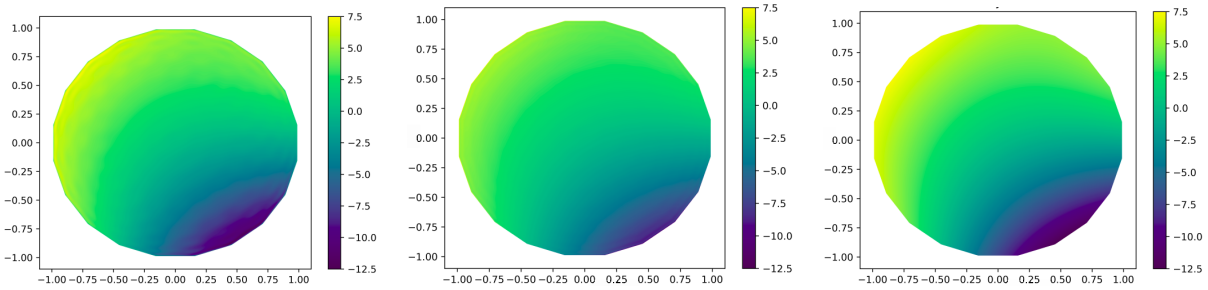

(a) Analytical function **(b) K basis approximation** **(c) Z basis approximation**

Figure 5. Difference in K and Z bases compared to the analytical function on an icosagon.

Although the Z basis approximation more closely agrees with the analytical solution, the K basis approximation has an error an order of magnitude lower than the Z basis. Graphically, the Z basis is also further than the K basis from the analytical function – the K basis is almost indistinguishable from the analytical function.

Moving from graphical evidence to error comparison, the errors of each approximation for the five polygons tested are plotted in Fig. 6. Although the graphical comparisons are sufficient to declare the K basis as superior to the Z basis, Fig. 6 quantifies the extent to which the K basis is a better approximation. For every polygon tested, the K basis has an error between 1 and 2 orders of magnitude lower than the Z basis. Additionally, the K basis converges with additional Zernike radial orders while, using the Z basis, orders above 10 marginally reduced or did not reduce the error for all polygons except the icosagon.

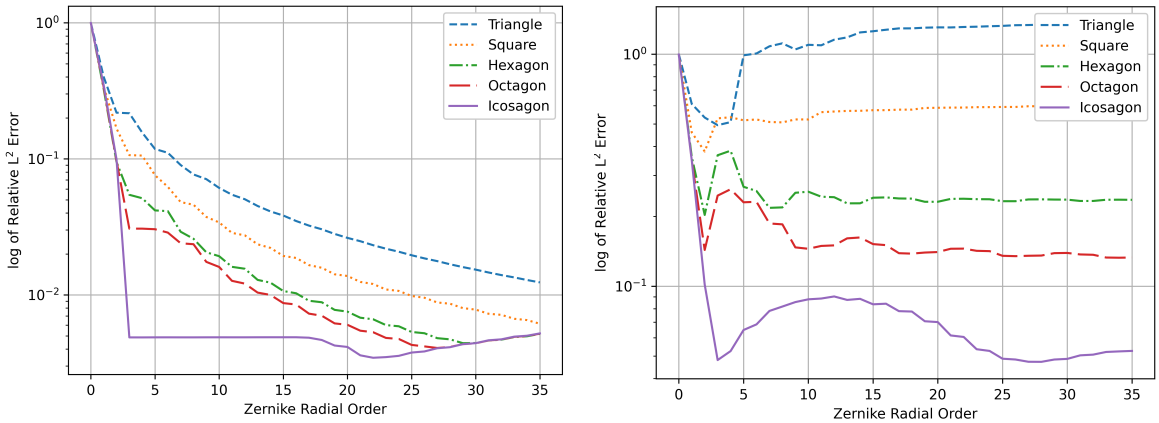

(a) K basis log scale **(b) Z basis log scale**

Figure 6. Difference in relative L^2 norm of Z and K basis approximations for different polygons.

However, the error for the K basis increases for higher Zernike radial order on the hexagon, octagon, and icosagon. The increase in error is due to a coarse numerical integration – the number of mesh bins M for each polygon was 5000. For these polygons, M was too low to avoid the discretization error being larger than truncation error for the higher order approximations. Although the error increases for certain K basis approximations, the increasing error is further proof that K basis is superior than the Z basis over polygons. The increasing error for the K basis only occurs when discretization error became the dominant effect. Conversely, with the values of M tested, the Z basis error is, at the minimum, an order of magnitude too high for the increase in discretization error to override the decrease in truncation error.

Additional testing for other smooth functions yields the same general conclusions – the K basis approximates the given function better than the Z basis over the polygon. The overwhelmingly positive results from this proof-of-concept motivates the implementation of polygon FETs into OpenMC.

4. OPENMC POLYGON FETs AND TEST PROBLEMS

The overwhelmingly positive proof-of-concept results motivates the implementation of polygon FETs into OpenMC. A short description on the OpenMC implementation is given in this paragraph. To use polygon FETs, a new parameter is added to the python API of the *ZernikeFilter* class. *ZernikeFilter* now accepts a parameter specifying the number of sides, set to 0 by default – the default value of 0 corresponds to the existing Zernike FET, so no changes are made to current functionality. If the number of sides corresponds to a three or more sided polygon, the transformation from Eq. 5 maps the regular polygon coordinates onto the unit disk. The transformed coordinates are then passed into the existing Zernike FET calculations. With this, polygon FETs are implemented in OpenMC.

With their implementation into OpenMC, the polygon FETs are benchmarked against existing distributed tallies. The model used for assessment is pictured in Fig. 7, and consists of a single, simplified Advanced

Burner Reactor (ABR) [5] fuel assembly with additional components on the periphery of the assembly. We stress that this test problem is manufactured to induce meaningful gradients in power across a hexagonal geometry, and is not representative of any real system. The remainder of the model is filled with water from (-20 cm, -20 cm) to (20 cm, 20 cm).

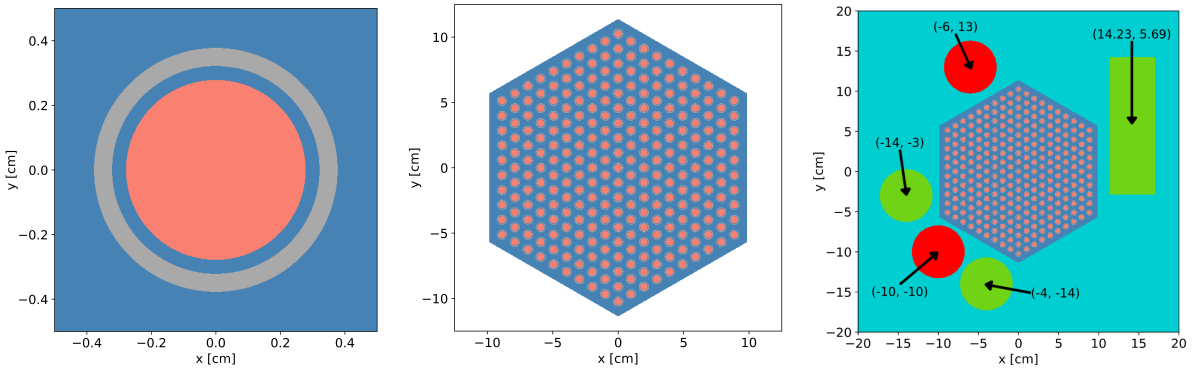

(a) Individual pin cell **(b) Fuel assembly** **(c) Entire model**

Figure 7. Model geometry.

The fuel assembly is composed of individual pin cells (Fig. 7a) surrounded by HT-9 steel cladding. The remainder of the fuel assembly is filled with sodium. The fuel pellet is composed of 15.5%$_{at}$ Pu and 84.5%$_{at}$ naturally enriched U. For specifications on the dimensions of the fuel assembly elements, see the ABR reference concept [5]. Outside of the fuel assembly, there are three groups of peripheral elements: a block of Pu in the top right, a single cylinder of boron in the top left, and a cluster of three cylinders in the bottom left. In the cluster with three cylinders, the outside cylinders are composed of Pu and the central cylinder was composed of boron. The block of Pu has a height of 14.23 cm and a width of 5.69 cm while each cylindrical element has a radius of 3.29 cm.

5. RESULTS

A branch of OpenMC with the polygon FETs is run with three tallies: (i) a distributed cell tally over the assembly lattice positions, to serve as a reference solution; (ii) an existing Zernike FET circumscribing the fuel assembly; and (iii) a polygonal Zernike FET perfectly aligning with the fuel assembly. Two scores are explored – a kappa-fission score in Fig. 8 (recoverable energy release) and a flux score in Fig. 9. The maximum relative error in the kappa-fission and flux distributed cell tallies is 1.7% and 0.04%, respectively. The third and fifth images show the FETs averaged onto the same domain as the distributed cell tally, for a 1:1 comparison. The color scales in these plots are shown in un-normalized form.

Both polygon and Zernike FETs have oscillations in the central region of the lattice for the kappa-fission score in Fig. 8. These oscillations manifest as concentric rings around for the polygon FET and a concentric ring of points for the Zernike FET – each ring is concentric about the origin. Additionally, the Zernike FET has lower values than expected around the periphery. Visually, there is no discernible difference between the Zernike FET and the distributed cell reference tally for the flux score. However, the polygon FET has distinct depressions bounded by the polygon radii, likely due to the "webbing" effect with the non-uniform sampling of space when mapped into the polygon coordinates.

The error, computed as $|u - u_*|/u_*$, where u_* is the reference tally and u is the FET averaged onto the distributed cell domains (small hexagons), is shown in Fig. 10. The polygon FET performs better than the

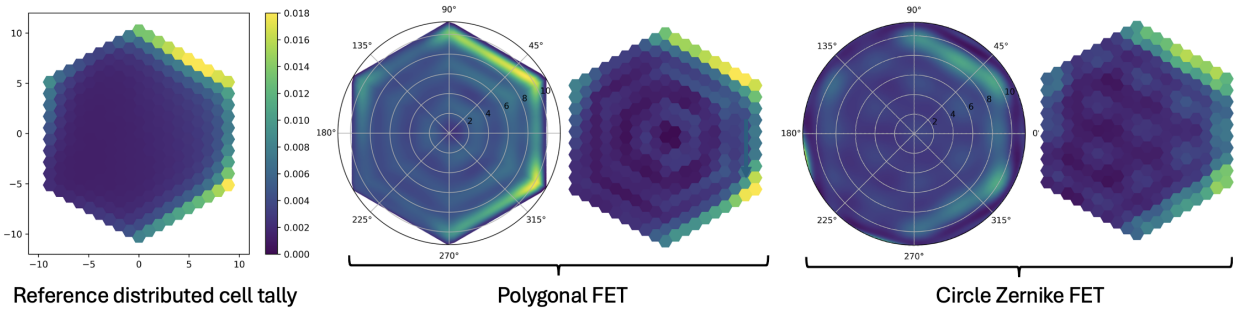

Figure 8. Comparison of tallies for `kappa-fission` score.

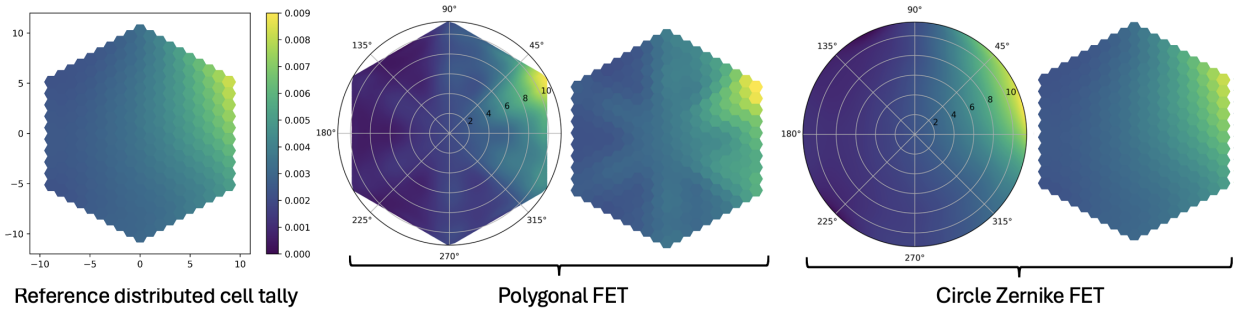

Figure 9. Comparison of tallies for `flux` score.

circular FET for the kappa-fission score, but worse for the flux score. This is likely due to two effects. First, the true kappa-fission distribution is not smoothly continuous through space (and has zero contributions to the circular FET in regions along the periphery of the circle). This likely imposes higher-order requirements on the FET needed to capture this profile, for which the polygon FET performs better. However, for the flux score, the distribution is smooth in space and there is no zero-contribution region for the conventional Zernike tally. In this scenario, then, the "webbing" arising from the non-uniform spatial mapping of points when converting from x, y to ρ, θ space likely causes the pattern of error observed.

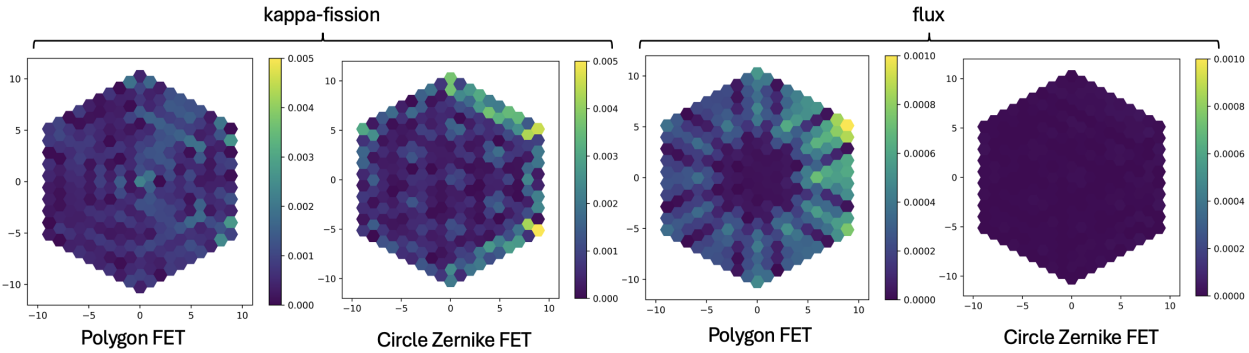

Figure 10. Error in the FETs, relative to a reference distributed cell tally.

Table I summarizes the maximum and average difference for the different FETs, relative to the distributed cell tallies. Several additional areas of investigation are needed before being able to make broad generalizations

about the efficacy of polygonal FETs. First, we plan to incorporate techniques to discard coefficients based on relative error. Second, a smoother mapping from x, y to ρ, θ space may alleviate the "webbing" observed in the polygonal basis functions, to improve smoothness. Future work will also include studies on computational performance, which should ultimately be the deciding factor in tally filter adoption.

Table I. Maximum and average error between reference distributed cell tally and each FET.

Score	Polygon Max.	Zernike Max.	Polygon Avg.	Zernike Avg.
kappa-fission	2.701×10^{-3}	5.627×10^{-3}	6.725×10^{-4}	8.786×10^{-4}
flux	1.085×10^{-3}	3.383×10^{-5}	2.336×10^{-4}	7.433×10^{-6}

6. CONCLUSIONS

In this paper, polygon FETs are introduced as an alternative to existing tallies. These polygon FETs provide a low-effort, accurate method for tallying polygonal geometries. A proof-of-concept is performed on different polygons with different functions and all results demonstrate the polygonal Zernike polynomials outperform the standard Zernike polynomials (should an analyst still attempt to use FETs on a non-orthogonal domain without the types of transformations used in this work).

Polygon FETs were then implemented into a branch of OpenMC. A toy problem used to compare distributed cell tallies, Zernike FETs, and polygon FETs. Polygonal FETs seem to perform better than conventional FETs when the tally distribution has sharp discontinuities, like the kappa-fission score. Higher errors for smooth distributions, like flux, suggest that additional effort be dedicated to developing a smoother spatial mapping routine to mitigate the "webbing" observed in the polygonal FET basis functions. Further testing is needed to explore additional polygon shapes and quantify computational performance. One possible future use case is to high-order tallies on general unstructured meshes.

REFERENCES

[1] P. K. Romano, N. E. Horelik, B. R. Herman, A. G. Nelson, B. Forget, and K. Smith. "OpenMC: A State-of-the-Art Monte Carlo Code for Research and Development." (2015). URL https://doi.org/10.1016/j.anucene.2014.07.048.

[2] P. D. Griesheimer. *Functional expansion tallies for Monte Carlo simulations*. Ph.D. thesis, University of Michigan (2005).

[3] B. Nijboer. *The Diffraction Theory of Abberations*. Ph.D. thesis, University of Groningen (1942).

[4] C. Ferreira, J. L. López, R. Navarro, , and E. P. Sinusía. "Zernike-like systems in polygons and polygonal facets." (2015). URL https://doi.org/10.1364/AO.54.006575.

[5] "Advanced Burner Reactor 1000MWth Reference Concept." Technical report, Argonne National Laboratory (2007).